An overview of the oxidation of Ni-based superalloys for turbine disc applications

Taylor, Mary; Cruchley, Sam; Evans, Hugh

DOI:
10.1080/09603409.2016.1171952

Document Version
Peer reviewed version

Citation for published version (Harvard):
Taylor, M, Cruchley, S & Evans, H 2016, 'An overview of the oxidation of Ni-based superalloys for turbine disc applications: surface condition, applied load and mechanical performance', *Materials at High Temperatures*, vol. 33, no. 4-5, pp. 465-475. https://doi.org/10.1080/09603409.2016.1171952

An overview of the oxidation of Ni-based superalloys for turbine disc applications: surface condition, applied load and mechanical performance.

S. Cruchley, H.E. Evans and M.P. Taylor*

School of Metallurgy and Materials, University of Birmingham, Birmingham, B15 2TT, UK

*Corresponding author: m.p.taylor@bham.ac.uk

Keywords: oxidation, Ni-based superalloys, gas turbine engines, shot-peening, fatigue.

Abstract

In this review the role of oxidation of chromia-forming Ni-based superalloys used for rotor disc applications in gas turbines is examined. A detailed review of the oxidation performance of these alloys in air is undertaken with emphasis on oxide composition and kinetics. The actual surface condition of the component entering service is important but often overlooked during oxidation studies. The effect of shot-peening on the oxidation of Ni-based superalloys is here evaluated. The oxide growth rates and composition of these alloys was assessed with respect to their response to an applied load or stress. One area where a significant amount of research has been conducted is on the effect of oxidation on the mechanical performance, with oxidation having been shown to reduce time to crack initiation, increase fatigue crack growth rates and therefore reduce overall component fatigue life. It is argued that this enhancement in crack growth rates arises from the cracking of an oxide intrusion ahead of the crack tip, exacerbated by Stress-Aided Grain Boundary Oxidation (SAGBO).

Introduction

Ni-based superalloys have been optimised, compositionally and microstructurally, to operate in the highly stressed conditions occurring in the hot sections of gas turbine engines. Under such conditions degradation by oxidation occurs and plays a key role in determining the lifetimes of the components. For this reason it is important to understand the oxidation processes occurring and the mechanisms involved. Most oxidation studies, especially those on Ni-based superalloys, are performed on specimens having a ground or polished surface rather than the actual condition the component would have entering service, in particular shot-peening, and it is important to quantify the effect this may have. Additionally, studies have primarily focussed on the study of oxidation without the application of an external load. This may be an important omission since in the real life operating conditions of these alloys, and the components they will be used for, significant external stresses can be present. This overview will examine the basic oxidation properties of chromia-forming Ni-based superalloys, the influence of surface conditions on these and oxidation/mechanical properties interactions.

Oxidation of chromia-forming Ni-based superalloys in air

Typical chemical compositions of various examples of this important group of γ′ (nominally, $Ni_3(Al,Ti)$) strengthened alloys are given in Table 1. Of relevance to oxidation properties, they are usually characterised by Cr contents in the range 13-20 wt.%, Al of 0.5 to 3.5 wt.% and Ti of 0.75 to 5 wt.%. Peak operating temperatures are unlikely to exceed 800°C.

Composition (% wt)	Ni	Co	Cr	Mo	Ti	Al	Ta	Hf	Zr	C	B	W	Nb	Fe
Udimet 720 Li	Bal	15.0	16	3	5	2.5	-	-	0.05	0.025	0.018	1.25	-	-
Astroloy	Bal	17	15	5.3	3.5	4	-	-	-	0.06	0.03	-	-	-
Waspaloy	Bal	13.6	19.3	4.2	3.6	1.3	-	-	0.05	0.01	0.04	-	-	-
ME3	Bal	18.2	13.1	3.8	3.5	3.5	2.7	-	0.05	0.03	0.03	1.9	1.4	-
IN718	Bal	-	19	3	0.9	0.5	-	-	-	0.04	-	-	5.1	18.5
Rene 95	Bal	8.0	14.0	3.5	2.5	3.5	-	-	0.05	0.03	0.01	3.5	3.5	-
RR1000	Bal	18.5	15	5	3.6	3	2	0.5	0.06	0.03	0.02	-	-	-
IN718 plus	Bal	9.1	18	2.7	0.75	1.45	-	-	-	0.02	0.005	1.0	5.4	9.5

Table 1: Compositions of some representative alloys [1-4].

The oxidation behaviour of several of these alloys has been studied extensively in air, e.g. IN718, RR1000, Udimet720, ME3, etc. [5-19] using both isothermal and cyclic oxidation tests. In general, the oxide scale formed is usually duplex consisting of a dense chromia (Cr_2O_3) layer and an outer layer of rutile (TiO_2) and a sub-surface internal oxidation zone (IOZ) of alumina (Al_2O_3), often consisting of acicular intergranular penetrations [5, 16, 18]. The IOZ is associated with a γ′ denuded zone, caused by Al depletion, that extends further into the alloy. Other surface oxides are often seen, e.g. NiO and CoO, and are often associated with early-stage transient oxidation. The newer more compositionally complex alloys, such as RR1000 and ME3, demonstrate most of these features as shown in Figure 1 but even in earlier, simpler alloys, e.g. Waspaloy, Astroloy and Udimet 720, internal oxidation of Al remains a dominant feature [5]. Both RR1000 and ME3 have each been reported to produce a new previously unseen oxide at the external oxide/alloy interface, with (Ti, Ta)O_2 being reported in RR1000 [17] and (Ta, Cr)O_2 in ME3 [15]. Of those alloys listed in Table 1, these are the only ones to contain Ta.

In addition to this new oxide, the external oxide/alloy interface becomes more complex with exposure time, developing protuberances and metallic regions within the oxide (e.g. Figure 1). This may be a

result of undercutting by oxide formation [20] or through outward alloy creep to accommodate the increase in volume from internal oxidation [21-25].

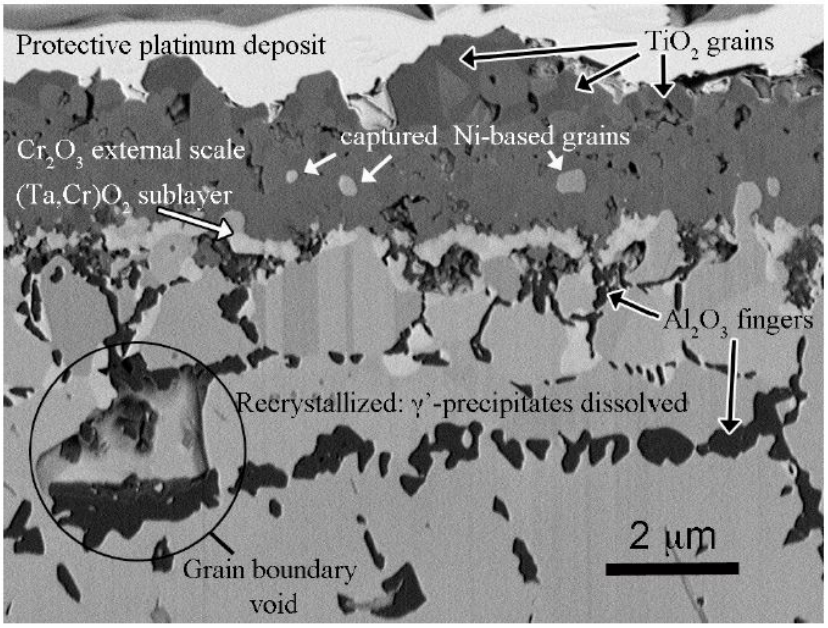

Figure 1: Oxidation of Ni-based superalloy, ME3, exposed to air at 815°C for 2020 hours, showing a surface layer of Cr_2O_3 with an internal oxidation zone of Al_2O_3 [15]. See text for fuller discussion.

Underneath this surface oxide, as mentioned previously, internal oxides and a γ′ particle free zone develop. Within this region recrystallisation, or perhaps simply grain growth, has been reported in both ME3 (Figure 1) and RR1000, although this has only been found in the fine-grained not the coarse-grained variant of the latter [7, 15, 26]. To add further complication, at particularly high temperatures (e.g. ≥850°C), particles of TiN have been shown to form ahead of the IOZ [14].

Furthermore it has been reported that within and ahead of the internally oxidised region, due to the depletion of Cr to the external oxide scale, is a zone of Cr-rich phase dissolution [15, 18]. Beneath this layer, remote from the oxide scale the grain boundaries are decorated with $M_{23}C_6$ precipitates (nominally $(Cr,Mo)_{23}C_6$) [15, 18]. MC carbides reside on the majority of the grain boundaries in the as-received alloy and decompose during high temperature exposure to $M_{23}C_6$. It is possible that Cr and Mo rich sigma (σ) phase (nominally $(Ni,Co)_x(Cr,Mo)_y$) could also form notionally as [27]:

$$MC + \gamma \rightarrow M_{23}C_6 + \gamma' \quad (1)$$

$$MC \rightarrow M_{23}C_6 + \sigma \quad (2)$$

In principle, the dissolution of such precipitates could lead to void formation [28] and initial work suggested [7] that sub-surface voids were present in oxidised RR1000, albeit attributed to vacancy injection [e.g. 29]. Later studies [30] have confirmed that the apparent voids were indeed sub-surface oxide particles. Nevertheless, some voidage has been observed in these alloys, as shown in Figure 1, but the possibility cannot be neglected that the example shown results from preparation damage, i.e. the loss of a small grain.

Most oxidation studies of these alloys have assessed the reaction kinetics using mass change measurements. The oxidation kinetics tend to be well described as parabolic and, as Figure 2 demonstrates, broadly similar parabolic growth kinetics are found [5, 7, 11, 12, 14, 16, 17]. Here, k'_p is the parabolic rate constant evaluated from the mass gain, (Δm) after oxidation time 't' as:

$$k_p' = \frac{(\Delta m)^2}{t} \tag{3}$$

The best-fit line through all the data in Figure 2 gives an Arrhenius expression for k'_p of:

$$k'_p = 5.68 \times 10^6 \exp\left[-\frac{281329}{8.314T}\right], \text{ mg}^2\text{cm}^{-4}\text{s}^{-1} \tag{4}$$

here *T* is temperature in K.

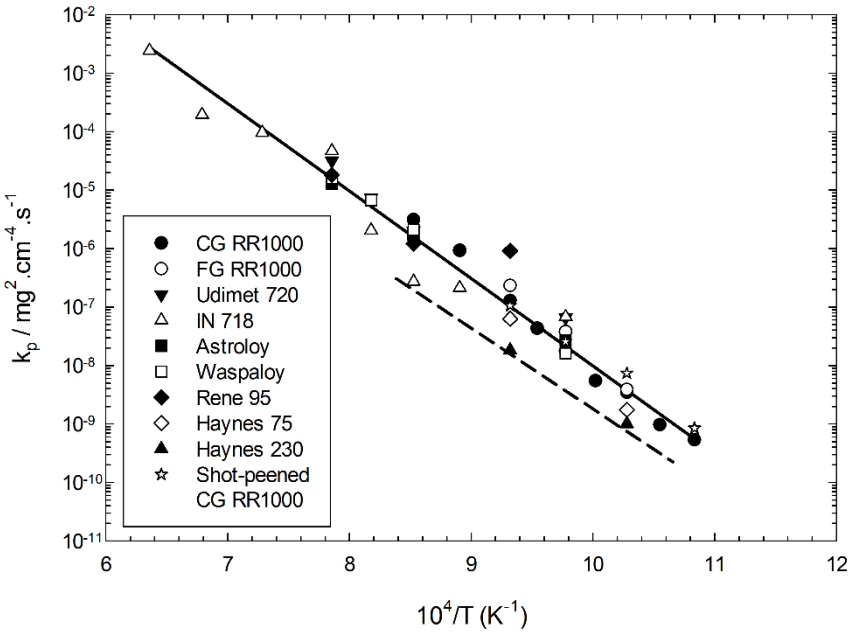

Figure 2: Arrhenius plot of kp values from the literature of similar Ni-based superalloys used for rotor disc applications [5, 7, 11, 12, 31, 32] and typical expected behaviour for chromia formation on a high chromium containing austenitic stainless steel (dashed line) [29]. Image modified from Cruchley et al. [14] to include data taken from [17].

This value of activation energy seems appropriate for all the relevant alloys shown but it is clear that there exists some scatter of values of the parabolic rate constant shown in Figure 2. The obvious, and most robust of these, is that the temperature dependence of the oxidation rate of the alloys is broadly similar to that observed for pure chromium and chromia-forming simple austenitic steels [29, 33] (the dashed line in the figure). This line also forms a lower bound to the superalloy data. Within the spread of these data, there also appears to be a trend that alloys low in Ti and/or Al (e.g. IN718, Haynes 75 and Haynes 230, show improved behaviour than the other superalloys. This is not unexpected since reactive elements such as Ti and Al are also being oxidised [e.g. Figure 1] and will contribute to the mass increase. As will be shown below, however, for RR1000, the chromia thickening rate was also substantially increased and, it will be argued, that this is a direct influence of Ti doping of the chromia layer.

A more informative method of evaluating reaction kinetics is through extensive metallographic measurements of oxide thickness, morphology and type and this has been undertaken recently for RR1000 [14, 17]. In this work, particular attention was paid to the chromia layer and its thickening with exposure time. The kinetics of chromia growth on polished specimens at 750^{o}C are shown in Figure 3 where a significant enhancement in the chromia growth rates over chromia formation on an austenitic steel and chromium was found. Sub-parabolic growth kinetics were found for the polished condition at 700 and 750^{o}C and near parabolic growth at 800^{o}C. The lower solid line in Figure 3 represents the best-fit through data obtained for chromia growth on a Ti-free austenitic steel (20Cr25Ni,Nb-stabilised) and for adherent layers on pure chromium [33] and given by:

$$k_p = 2.07 \times 10^{-6} \exp\left[-\frac{31020}{T}\right],\ m^2s^{-1} \qquad (5)$$

Here, T is temperature in Kelvin, the parabolic rate constant, k_p, is expressed in terms of thickness, ξ, of the chromia layer as:

$$k_p = \frac{\xi^2}{t} \qquad (6)$$

where t is exposure time.

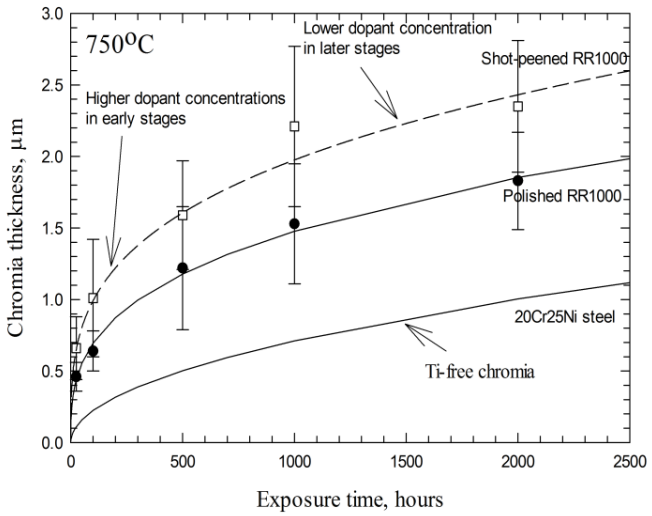

Figure 3: Plot of chromia thickness measured on RR1000, with and without shot-peening, at 750°C compared with Ti-free austenitic steel/pure chromium. Oxide measurements for both conditions were normally distributed and error bars are shown as ± 1 standard deviation. Hollow squares are measurements for shot-peened RR1000, filled circles are polished RR1000 [17].

SEM/EDX examination of the chromia layer in the above specimens has shown that substantial quantities of Ti are present in solution, not associated with TiO_2. The ability of chromia to dissolve Ti, probably with a valency >3, has been known for some time (e.g. [34, 35]). A possible defect reaction suggested by Atkinson and co-workers [35, 36] envisages a 4-valent Ti ion entering the chromia lattice according to:

$$3TiO_2 \rightarrow 3Ti_{Cr}^{\cdot} + V_{Cr}^{'''} + 6O_o^x \qquad (7)$$

here $3Ti_{Cr}^{\cdot}$ represents the excess positive charge associated with the titanium ion located on a chromium lattice site, $V_{Cr}^{'''}$ is a triply charged Cr vacancy, O_o is the oxygen ion on the oxygen sub-lattice. The excess vacancies would increase the oxidation rates through the increased diffusion of chromium ions across the oxide layer. Sub-parabolic kinetics are thought to have developed as a result of the average quantity of Ti within the chromia layer decreasing as the layer thickens because of Ti depletion in the underlying alloy. As a consequence, the enhancement in growth rate reduces with exposure time and the kinetics tend to sub-parabolic rather than parabolic [14]. This trend of a decreasing enhancement in the growth rate of the doped oxide with exposure time is shown graphically in Figure 4(a) for polished RR1000 specimens and Figure 4(b) for shot-peened RR1000 specimens [17]. Here the enhancement factor is expressed by the ratio, r, of chromia growth rates in the superalloy (suffix S) to that of Ti-free chromia (suffix Cr) at a given oxide thickness in both cases:

$$r = \left[\frac{(d\xi/dt)_S}{(d\xi/dt)_{Cr}} \right]_\xi \tag{8}$$

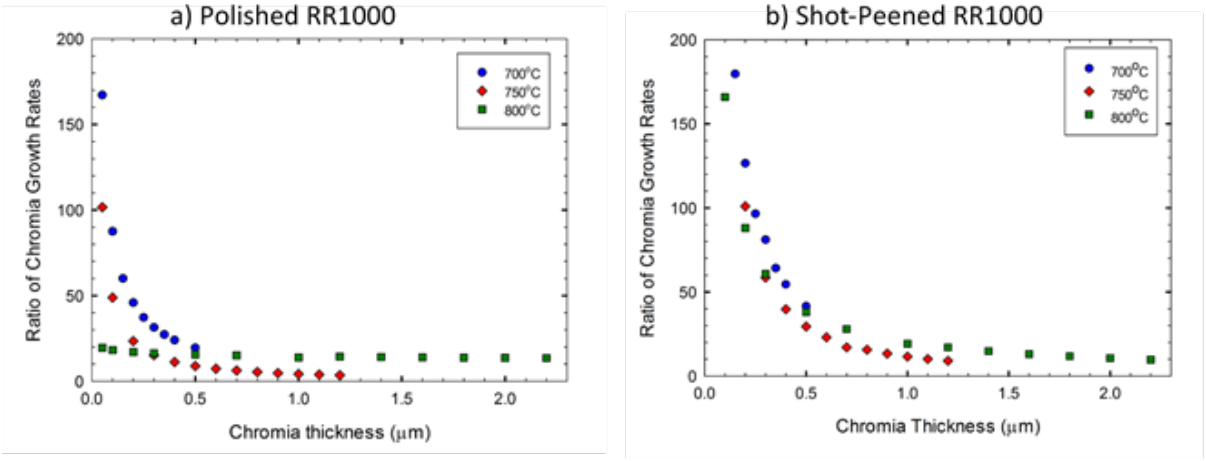

Figure 4: The variation of the enhancement ratio of the chromia growth rate due to Ti doping with oxide thickness for 700°C, 750°C and 800°C, in a) polished RR1000 and b) shot-peened RR1000 [17].

The enhancement ratio is high for thin oxides at 700 and 750°C on the polished specimens, indicating high dopant levels, but rapidly decreases with increasing oxide thickness. At 800°C, the enhancement is lower initially but remains reasonably constant with increasing oxide thickness. The reason for this is unclear but may be associated with the presence of a near-continuous layer of the $(Ti,Ta)O_2$ phase underlying the chromia scale. A consequence is that near-parabolic kinetics obtained at this temperature but not at the two lower temperatures shown.

A characteristic feature of the chromia-forming superalloys examined here is the presence of regions of sub-surface, oxidation-induced damage. The most striking of these is the formation of oxides of Al and Ti which can exist as acicular intrusions along alloy grain boundaries (Figures 1 and 5) as well as discrete particles within the alloy grains [18]. As will be discussed, the grain boundary oxides can influence the nucleation of surface cracks during mechanical testing. Internal oxidation of these alloys has been reported extensively [5, 9, 11, 13] but detailed measurements of kinetics are sparse. An extensive metallographic study has recently been performed by Cruchley et al. on RR1000 over the temperature range of 700-800°C for exposure periods up to 2000 hours in air [18]. This work showed that the intergranular and intragranular penetration rates were parabolic. The selective oxidation of Al and Ti results in the dissociation of the γ′ ($Ni_3(Al,Ti)$) precipitates in the near-surface regions and the formation of a precipitate-free zone (PFZ). The depth of this zone also increases parabolically with time [18].

Effect of shot peening

Surface finish and residual stress underneath the surface are controlled and modified to improve the mechanical properties of in-service components. Various studies have established that the oxidation behaviour of stainless steels, Ni alloys and Fe-Cr alloys are dependent on the surface finish prior to oxidation [37-47]. Relatively little work has been conducted, however, on the effect of surface condition on the oxidation of Ni-based superalloys where most studies have examined the ideal highly polished or as-received machined condition [5-7, 15, 48].

Shot-peening has been widely employed to improve the fatigue resistance of components by inducing significant surface compressive residual stresses [49, 50]. For the current chromia-forming superalloys, the effect of shot-peening on oxidation has only been investigated in detail in two studies on coarse-grained (30-50 μm) Ni-based superalloy, RR1000 [17, 19]. Testing in both cases was performed in air between 700-800^{o}C for up to 2000 hours. In this variant of RR1000 it has been reported that recrystallization of the near surface grains only occurs in the oxidised shot-peened condition [17], which is in contrast to the findings reported for the fine-grained variant of RR1000 (4-6 μm) and ME3 (27-30 μm) [7, 15, 26]. Such recrystallization can be expected to produce a surface region of different mechanical properties from that of the bulk alloy.

While no changes in oxide composition have been reported for shot-peened specimens, changes in morphology of the internal oxide and the γ′ PFZ have been observed, together with the development of a more planar front of internal oxidation (Figure 5) [17, 19]. This morphology appears to result from the finer grain size associated with the recrystallized zone (Figure 5b). At 800^{o}C, both the shot-peened and polished specimens developed (Ti, Ta)O_2 at the chromia/alloy interface although this occurred as isolated regions in the shot-peened condition compared with a near continuous layer in the polished condition [17].

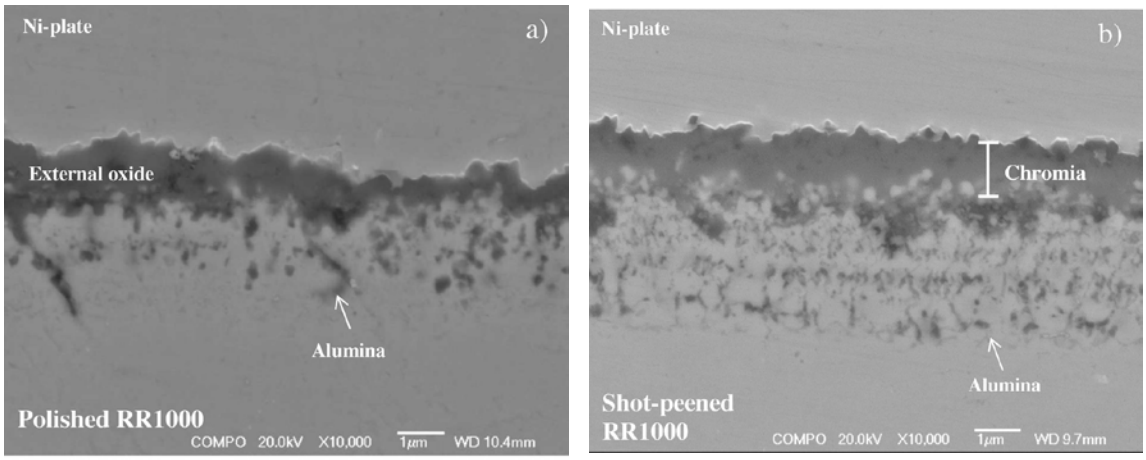

Fi **n a) polished RR1000 and b) shot-peened RR1000 oxidised** **s at 700°C [17].**

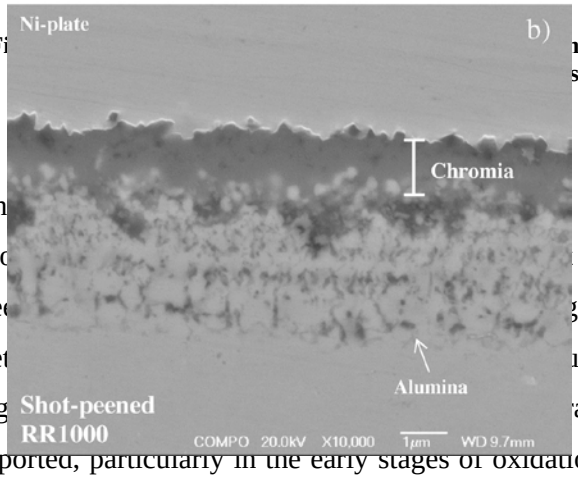

Th and shot-peened RR1000 alloy were found to be br being found at 700 and 750°C [19] for the shot-pe growth kinetics of the surface chromia layer as de urements [17]. As with the polished condition a sig rates over those expected for Ti-free chromia was reported, particularly in the early stages of oxidation. This is illustrated in Figure 4, using equations (5), (6) and (8). The behaviour is similar to that found for the polished condition (Figure 4a) except that the trend exists at 800°C also and this may be related to the non-continuous nature of the $(Ti,Ta)O_2$ phase at the chromia/alloy interface in the shot-peened specimens. As with the polished specimens, Ti doping of the chromia layer is thought to be responsible for the large rate enhancement. The decline of the enhancement ratio with increasing oxide thickness indicates that the chromia growth kinetics are sub-parabolic in the shot-peened specimens of RR1000 over the temperature range of 700-800°C.

An interesting study by Foss et al. [26] has investigated oxygen transport in fine-grained RR1000 at 800°C for 120 hours using a two stage isotopic exposure ($^{16}O_2$ for 72 hours followed by $^{18}O_2$ for 48 hours) at 200 mbar. Both polished and shot-peened surface finishes were examined but the general oxide morphology was similar in both and also to the results reported by Cruchley et al. [14, 17] on the coarse-grained alloy variant. A significant observation was that the surface chromia layer grew both by cation diffusion (new oxide formed on the outer surface of the layer) and by anion diffusion (new oxide formed at the oxide/metal interface). The growth of chromia by such counter-current diffusion is well established for layer growth on simpler alloys [51] so its demonstration on a complex superalloy with Ti-doped chromia is a helpful contribution. It shows that the doping is not

accommodated by significant defect changes on the oxygen sub-lattice, an expected reduction in oxygen vacancy concentration, but by the cation sub-lattice as indicated by the defect reaction (7).

Application of an applied load on oxide composition and growth

Studies of high temperature oxidation of metals have focussed primarily on oxidation composition and growth kinetics in the absence of an external load. This is an important omission since in service these materials, and the components they will be used for, often experience significant external stresses. This is especially the case with Ni-based superalloys which are designed to operate in the highly stressed regions of gas turbine engines. While the literature is limited, several studies have investigated the application of an external load, either compressive or tensile, on the oxidation kinetics of a number of alloy systems [26, 32, 52-57].

Studies in this area have often focussed on Ni and simple Ni-based alloys as this is the base metal/system used in most superalloys. For example, application of tensile stresses of 10 and 20 MPa have been shown to increase the weight gain due to oxidation of Ni at 700^{o}C whereas a stress of 6 MPa did not [52, 53]. This apparent critical stress could be associated with through-thickness cracking of the oxide scale which would be expected to increase oxidation rates. Its value can be estimated well enough from [58]:

$$\sigma_c = \left(\frac{K_{1c}}{f(\pi a)^{0.5}} \right) \tag{9}$$

Here the defect half-length, a, is measured perpendicular to the in-plane critical stress, σ_c, in the oxide layer. f is a geometric factor, ~1, and K_{1c} is the critical stress intensity factor. Measurements on NiO scale grown on Ni give K_{1c}=0.4 MPa.m$^{-½}$ at room temperature and 1.6 MPa.m$^{-½}$ at 900^{o}C [59]. The oxide layer thickness in the experiments of Zhou et al. [52] was ~3 μm so that the maximum defect length present was unlikely to be larger than 1.5 μm, i.e. a=0.75 μm. Using this value in equation (9) together with a mid-range value of K_{1c}=1 MPa.m$^{-½}$ and f=1 gives the critical stress as ~650 MPa, i.e. approximately 2 orders of magnitude larger than that reported by Zhou et al. [52]. This very large discrepancy was not addressed in the original papers but can be understood once it is appreciated that the stresses quoted by Zhou et al. seem to be those applied to the gross sectional area and not those necessarily present in the oxide layers. The specimens tested were composites consisting of an outer NiO layer and a Ni core. Prior to cracking of the oxide, i.e. up to a gross applied stress of ~6 MPa, both of these components will deform to the same uniaxial strain in order to retain continuity. In order to achieve this, the applied load will redistribute across the cross section according to [60, 61]:

$$2\sigma_{ox}\xi w + 2\sigma_s h w = 2\sigma_g (h + \xi) w \tag{10}$$

Here, the specimen of rectangular cross-section is oxidised on all surfaces to produce an oxide thickness, ξ, on the major flat surfaces. The core width is 2h and the specimen has thickness w. σ_g is the gross applied stress, σ_{ox} is the average in-plane stress in the oxide layer and σ_s is the corresponding average value for the core alloy. From equation (10), the average stress in the oxide layer is:

$$\sigma_{ox} = \left[\frac{\sigma_g(h+\xi) - \sigma_s h}{\xi} \right] \tag{11}$$

Higher stresses will be generated in the stronger component, in this case, the oxide layer which is expected to deform elastically. The Ni core, by contrast, will deform by creep at much lower stresses. It is beyond the scope of the present paper to undertake a detailed evaluation but a rough estimate of the oxide stress can be made. The tensile fracture strain of the oxide will be around 0.5% [59] which requires an in-plane tensile stress of ~875 MPa for a Young's modulus of the oxide at 700^{o}C of 175 GPa [62]. This value of stress is again very much larger than that applied to the entire cross-section but is consistent with that deduced from likely defect lengths through equation (9). Similar considerations apply to the tests undertaken in compression by Zhou et al. [52] where enhanced oxidation and the formation of fine-grained oxide was found for gross applied stresses of 20 MPa [52]. On the basis of the above arguments, actual in-plane compressive stresses in the oxide are likely to be of order 1 GPa and these may initiate oxide spallation. This was not reported by Zhou et al. but was found by Moulin et al. [54] under creep and creep/fatigue conditions.

It has been important to re-examine the results of Zhou et al. since their study provides a systematic investigation into the influence of stress on oxidation in the Ni/NiO system. Of concern was the possibility that significant deleterious effects could be produced at very low applied stresses which would be encountered readily in service. The above discussion, however, offers reassurance that, in fact, much larger stresses, of order 1 GPa, need to be applied to the oxide to produce the observed cracking and morphological changes. This issue of quantifying the magnitude of stress in the oxide layer is generic whenever testing is done using conventionally-shaped test specimens as used for uniaxial loading. As far as the present authors are aware, no allowance has been made in the available literature for the redistribution of load that occurs on testing the oxide/metal composite specimen. Nevertheless, when the core material is a strong superalloy of high creep strength and a high yield stress, e.g. $\geq$1GPa, the load-bearing capacity of both the core and oxide layer will be similar. The load distribution across the section will then not be large but should still be evaluated in order to obtain quantitative insights.

The published work on the superalloys clearly shows qualitatively an influence of applied stress on oxide morphology and section loss. An example, taken from the work of O'Hanlon et al. on fine-grained RR1000 [56], is shown in Figure 6. In this study, the effect of a static load was investigated at both 650°C and 700°C for 200 hours under compressive and tensile gross stresses of 300 and 600 MPa. Figure 6 shows examples of the oxide morphology developed at 600 MPa together with that under unstressed conditions (Figure 6b). It is clear that under both tensile (Figure 6a) and compressive (Figure 6c) stress, the protective surface oxide has been compromised, probably by cracking or local spallation, and regions of enhanced damage develop. A related study [55] on fine-grained RR1000 tested under tensile fatigue at 700, 750 and 800°C did not demonstrate enhanced thickening of the surface oxide although, at 800°C only, there appeared to be an enhancement of sub-surface attack at the peak tensile stress of 670MPa, at least at mean behaviour.

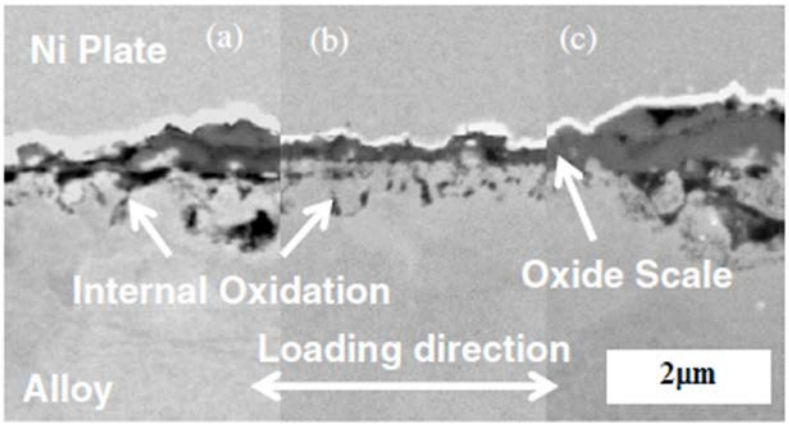

Figure 6: Backscatter electron images of oxidation damage on fine-grained RR1000 after 200 hours at 700 °C under hold stresses of (a) + 600MPa, (b) 0MPa and (c) −600MPa [56].

Various other studies on chromia-forming superalloys such as Udimet 720, ME3 [63], IN100 [57] have demonstrated that applied stress can affect not just oxide morphology and thickness but also the depth of internal oxidation and the γ′ depleted zone. These tend to show a deleterious effect at high stresses but not all results are consistent. In particular, a tensile stress (nominally, 133 MPa maximum) may promote the earlier beneficial formation of a chromia layer in Haynes 75 and 230 [32]. Interpretation of all these data is not straightforward because of the uncertainty in establishing actual oxide stress levels. The difficulty is compounded not just by the load redistribution discussed above but also by stresses developed by growth strains within the oxide layer. These can be negligible for the Ni/NiO system [64] but may be hundreds of MPa compressive for chromia scales [65].

The Influence of Oxidation on Crack Nucleation and Growth

Crack Nucleation

The alloys considered here usually experience systematic variations in stress during service and considerable research effort has been expended in attempting to understand their high-temperature fatigue behaviour under oxidising conditions. A recent overview of the topic has been provided by Pineau et al. [66]. It is not the intention to reprise this here but rather to focus on recent observations on oxidation effects on both crack nucleation and, in the next section, on crack growth.

An example of the oxide morphology that develops in these chromia-forming, Ni-based superalloys as a result of air exposure has been shown in Figure 1. As has been discussed, the oxides that form have low tensile fracture strains (< 1.0%) and low fracture toughness (0.4-2 $MPa.m^{1/2}$) [67]. It would then not be unexpected for oxide cracking, either surface or intergranular, to occur at local nett tensile stresses in the range 0.5-1.0 GPa [68, 69] and an example of this is shown in Figure 7 [68]. This specimen of RR1000 had been exposed without stress in air for 2000h at 700^{o}C and then fatigued (at R=0.1) under 4-point bend at room temperature at a maximum in-plane surface stress of 800 MPa. In the light of the earlier discussion, this calculated value of stress is probably reasonable since both the oxide and alloy will have deformed elastically and have similar load-bearing capacities. There remains uncertainty, unfortunately, in the oxide growth and thermal stresses that exist.

The micrograph of Figure 7 clearly shows the presence of cracking in both the surface chromia layer and the alumina sub-surface intergranular penetration. This crack has penetrated intergranularly into the alloy ahead of the oxidation front but within a presumably weak grain boundary zone depleted of γ′ precipitates and Cr-rich carbides. This zone develops as the result of the selective oxidation of Cr, Ti and Al and its depth should be considered in assessments of oxidation-induced damage.

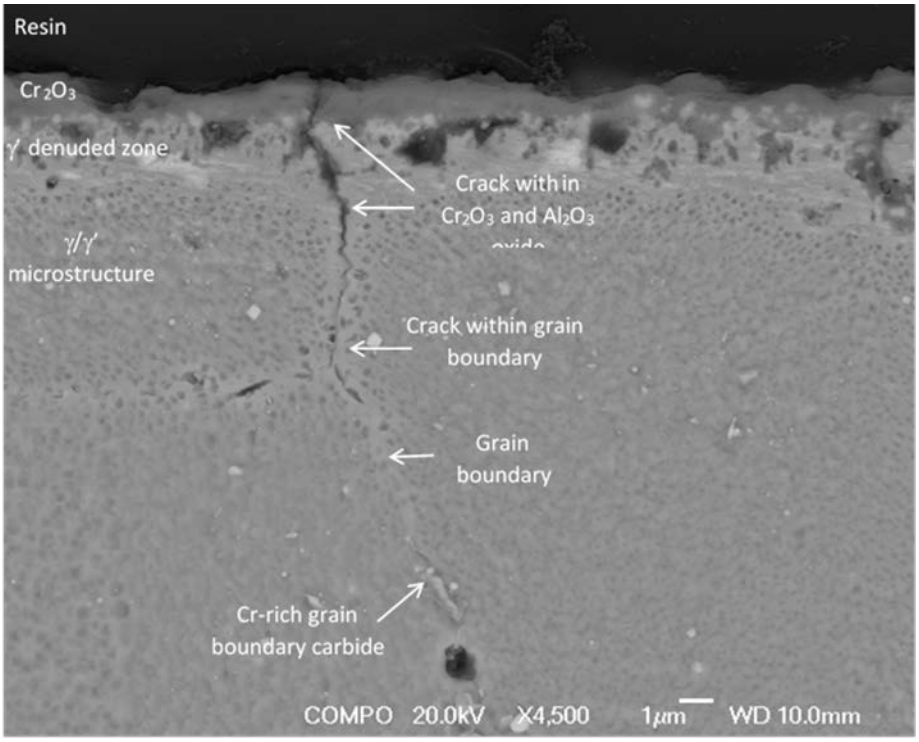

Figure 7: BSE image of an etched pre-oxidised (2000h, 700°C) specimen that failed after $1.9x10^6$ cycles during room temperature 4-point bend at a maximum applied stress of 800 MPa, showing cracking of the external and intergranular internal oxide along with the presence of both a γ′ denuded zone and carbide dissolution zone [68].

The importance of accounting for the presence of this zone is further demonstrated by the experiments of Sudbrack et al. [15] on ME3. Their results, summarised in Figure 8, show that prior high temperature exposures in an oxidising environment for exposure periods up to 2020 hours have a detrimental effect on the high temperature (704 and 815°C) notched fatigue life [15]. The thicker the external scale and the deeper the internal damage the more pronounced the reduction in life. The reduction in life in this case was driven by $M_{23}C_6$ carbide dissolution. Removal of the internally oxidised region did not lead to a complete recovery in high temperature fatigue life (~20μm) but the removal of the carbide dissolution zone (~50μm) did (Figure 8).

Another study using prior exposures on the Ni-based superalloys, ME3 (704°C for 439 hours) and Udimet 720 (650°C and 704°C for 100 or 1029 hours) found that the mean lives of pre-oxidised specimens had up to a 70% reduction in low-cycle fatigue (LCF) life. A change of crack initiation was also seen from sub-surface (as-received) to surface (pre-oxidised). Performing the prior exposures in vacuum led to no reduction in fatigue life, illustrating that oxidation damage is driving the reduction in life [63]. Pre-oxidation under an applied stress (97 MPa) has been shown to cause a further reduction in LCF life of the Ni-based superalloy, Rene 80, over both as-treated and unstressed prior oxidised (100 hours at 982°C) specimens. This is in addition to the reduction in life the

unstressed prior oxidised specimens recorded over the as-treated specimens [70]. Fatigue testing of the Ni-based superalloy, IN100, at 1000°C in an oxidising environment has been shown to drastically reduce the time to crack initiation compared with tests performed in vacuum. The crack initiation life was similar to the total number of cycles it took to fracture the oxide [57]. Similar observations of crack nucleation at oxidised grain boundaries have been reported recently on N18 [71] where it was also noted that the cycles to crack initiation formed the larger part of the total cycles to failure.

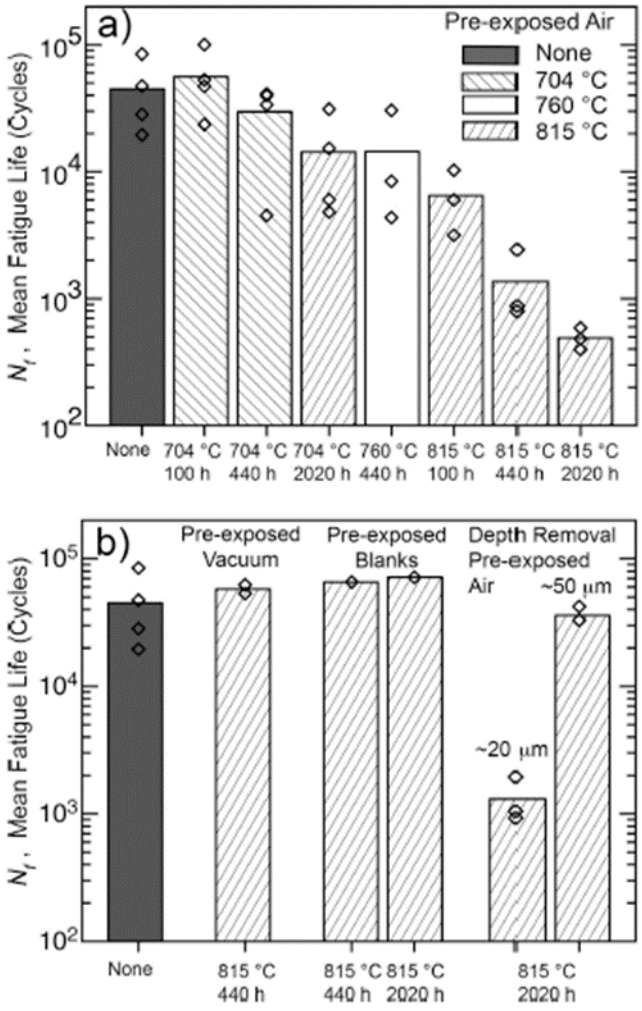

Figure 8: Comparison of the mean notched fatigue lives at 704 °C of the unexposed ME3 specimens and ME3 specimens with a) prior exposures in air and b) alternative conditions as marked. Diamonds are each test result, clearly showing that the removal of all of the environmental damage (50 mm removal) leads to a full restoration in fatigue life [15].

Further studies on RR1000 using prior exposure at 700°C have been shown to affect the high cycle fatigue (HCF) life significantly [68, 69]. Predominantly this was by reducing fatigue lives although exposed specimens were also observed to outperform the as-machined testpieces at stress levels around 825-900 MPa. This unexpected, beneficial effect of oxidation was attributed to local stress relaxation in the surface γ′-depleted zone associated with the selective oxidation of Al and Ti. The

yield stress of this zone was surmised to be around 825 MPa, i.e. substantially less than that (> 1 GPa) of the bulk alloy. At lower stresses, no relaxation took place and the cracking of surface oxides proved deleterious (Figure 7). At stresses > 900 MPa, crack propagation through the depleted zone occurred readily and again, prior oxidation proved deleterious. This is an intriguing result, in principle, but, as discussed above, further work is required to quantify the stress state in both the external oxide and the sub-surface internally oxidised region.

Crack Growth

Extensive evidence exists in the literature showing the deleterious effect of oxidising environments on high temperature dwell fatigue performance. Some of this is due to crack nucleation, as discussed above, but there is also a substantial increase in crack growth rates in the presence of oxygen [72-76] and a change in crack path from transgranular to intergranular, typically seen in low oxygen environments (vacuum/argon). An example of these features is shown in Figure 9 [76] for the LHSR alloy (12.5 Cr, 20.7 Co, 2.7 Mo, 4.3 W, 3.5 Ti, 3.5 Al, 1.6 Ta, 1.5 Nb, bal. Ni, wt.%) tested at 650 and 725^{o}C in either air or vacuum with single notched specimens under 3-point bending. A general feature of such plots is that the crack growth rate decreases sharply as some notional threshold ΔK_{th} or K_{th} is approached. The threshold value is lower in air than in vacuum.

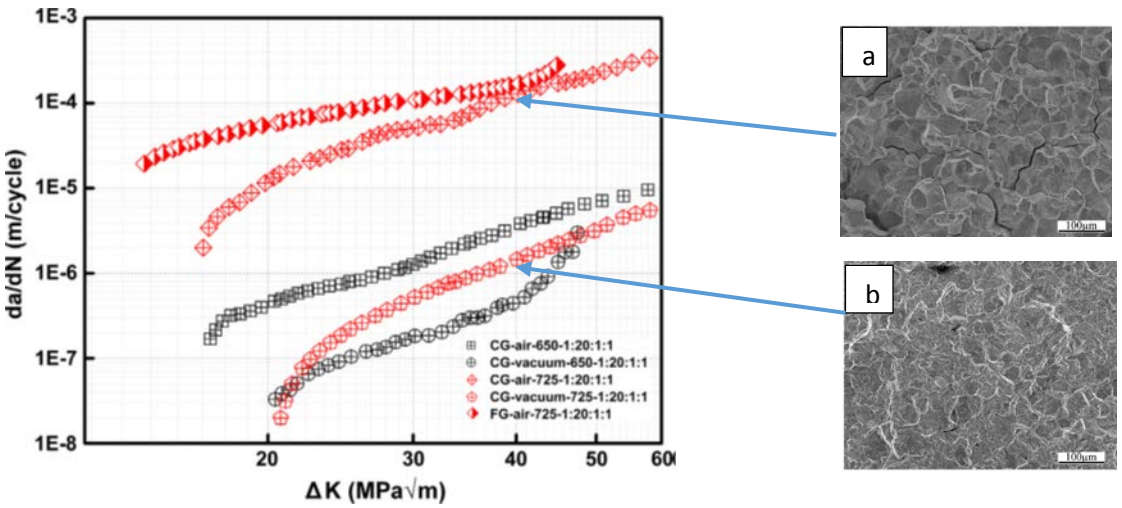

Figure 9: Main graph shows crack growth rates versus ΔK in the LHSR alloy tested under 3-point bend at 650^{o}C (black symbols) and 725^{o}C (red symbols) under air and vacuum. Increased rates were observed in air at both temperatures but were greater at the higher temperature. Micrograph (a) shows the intergranular fracture behaviour at 725^{o}C in air and (b) the transgranular behaviour in vacuum both at ΔK~40 MPa.m$^{-½}$ [76].

Much effort has been expended in attempts to understand the deleterious role of oxygen on crack growth but the process remains incomplete although two contending mechanisms currently dominate thinking. The dynamic embrittlement model envisages that elemental oxygen diffuses into the alloy

grain boundary from the crack tip and produces cohesive weakening [77-79] in a manner analogous to S embrittlement. The concept is influenced by the experiments of Bricknell and Woodford [80, 81] on Ni containing different amounts of carbon exposed to oxidising and non-oxidising environments at 1000^{o}C. In impure Ni, oxidation of the C content occurred under oxidising conditions even though Ni oxidation was prevented and extensive bubbles of CO_2/CO were produced together with significant embrittlement at 800^{o}C. In the purest grade of Ni examined, few if any bubbles were present but substantial embrittlement still occurred suggesting (but not by Bricknell and Woodford) that intergranular cohesive weakening arose in the presence of dissolved elemental oxygen. These experiments were well conducted but the extrapolation of their findings to complex Ni-based superalloys should be undertaken with much caution. The erroneous feature of the argument is the assumption that elemental O could exist in such alloys at sufficient concentration to cause intergranular embrittlement in the presence of elements such as Cr, Ti and Al that have a strong affinity for O. As an example, the reaction between O and Cr would reduce the fractional partial pressure of O in equilibrium with chromia to as low as ~10^{-32} at 650^{o}C [82]. Chemical reaction to form oxides of these elements is much more energetically favoured than O segregation to the alloy grain boundaries and this forms the basis of an alternative mechanism of enhanced crack growth under oxidising conditions.

In this second model, it is envisaged that oxides of low fracture toughness form at the crack tip and penetrate along the alloy grain boundary ahead of it. Crack advancement occurs by the subsequent repeated cracking and reforming of these brittle oxide intrusions [83, 84]. Recent atom probe tomography and TEM studies support the presence of oxides penetrating the alloy from the crack tip [82, 85, 86]. An example of these oxide wedges, observed with TEM [82], is shown in Figure 10 for RR1000 tested at 625^{o}C. This particular image shows the tip of the intrusion and the thermodynamic sequencing of the oxide layers that exists within it. By this is meant that oxides of lower thermodynamic stability, in this case CoO and NiO, are present at the central regions of the inclusion whereas the most stable oxides such as alumina and rutile are present adjacent to the alloy surface. Similar observations have been reported by Viskari et al. [86]. This is an unexpected result that indicates that individual layers can reduce the partial pressure of oxygen beneath them to their equilibrium dissociation pressure.

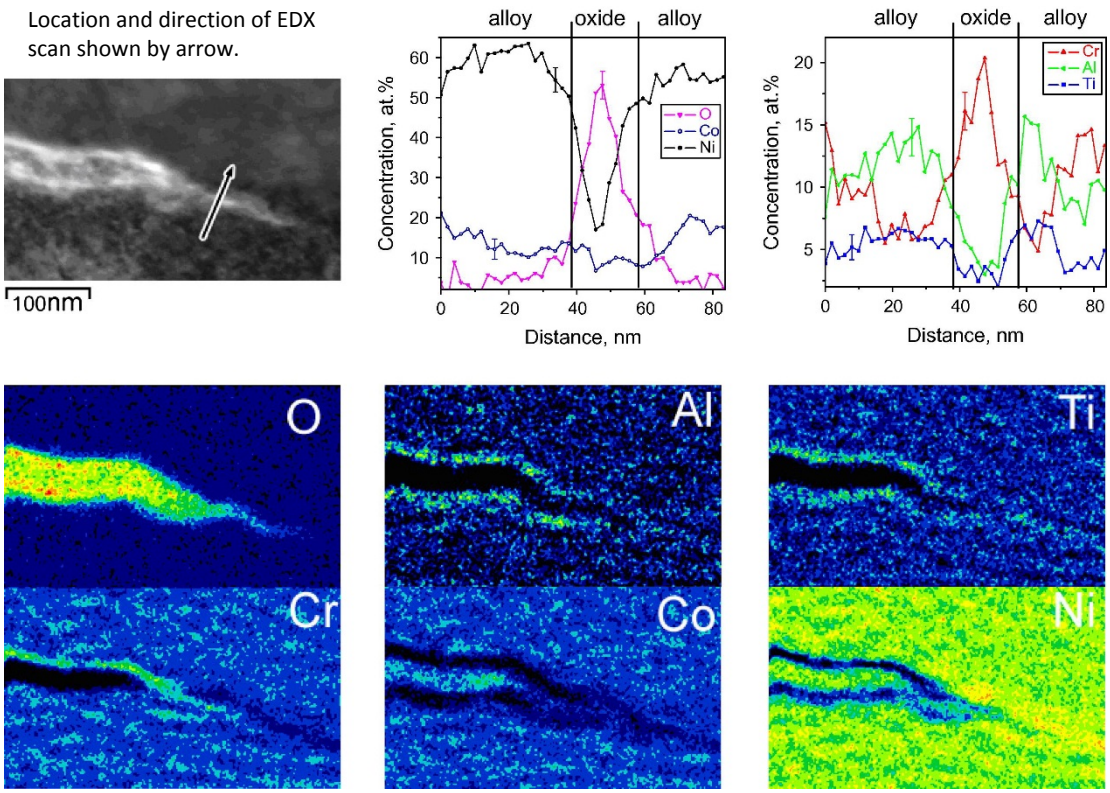

Figure 10: A bright field STEM image, EDX maps and linescans obtained ahead of the crack tip in RR1000, illustrating the presence and sequence of oxides. The relative concentration in the EDX maps increases from low to high in the sequence: black, blue, green, yellow, orange and red [82].

The principal oxides found by Kitaguchi et al. [82] that existed along the intrusion were NiO or Cr_2O_3 (chromia) depending on the detailed test conditions. In each case, the intrusion lengths were appreciably longer than would be expected, e.g. enhancement factors of ~17.6 for chromia and ~3.6 for NiO. This enhancement was considered to be a result of Stress Aided Grain Boundary Oxidation (SAGBO). The model of SAGBO that was developed [87] recognises that oxide formation will generally lead to an increase in volume and that this volumetric strain at the crack tip will fundamentally change the local stress distribution there. For loading conditions less than or of order that required for crack advance, i.e. near the threshold condition, K_{th} or ΔK_{th}, the normal stress at the crack tip will be compressive but will become less so with increasing distance from the crack tip and will be tensile at the tip of the wedge-shaped oxide intrusion [87]. This tensile stress leads to an increase in the outward flux of oxygen vacancies, and a corresponding increase in the inward diffusion of oxygen along the intrusion, producing an increase in oxide growth rate.

The ratio of growth rates of the intrusion of the stressed state to unstressed condition is given by the SAGBO enhancement factor, S_r, defined as [87]:

$$S_r = \left(\frac{\left(\dot{\ell}\right)_\sigma}{\left(\dot{\ell}\right)_o} \right) = \exp\left(\frac{\sigma_{it}\,\Omega_M(\Phi - 1)}{kT} \right) \qquad (12)$$

Here, σ_{it} is the normal stress at the intrusion tip, k is Boltzmann's constant, T is absolute temperature, Ω_M is the volume of a metal atom in the alloy, calculated from molar volumes as 1.10×10^{-29} m^3 for Ni and 1.22×10^{-29} $m^3$for Cr. The term (Φ-1) represents the factor increase in metal volume on oxide formation. There is some uncertainty in the values to be used for Φ but taking those for the Pilling-Bedworth ratio is likely to introduce relatively little error for NiO and chromia. The calculated values of S_r at 650°C (923K) with Φ = 1.65 for NiO and = 2.07 for chromia are shown in Figure 11 as a function of the normal stress at the intrusion tip.

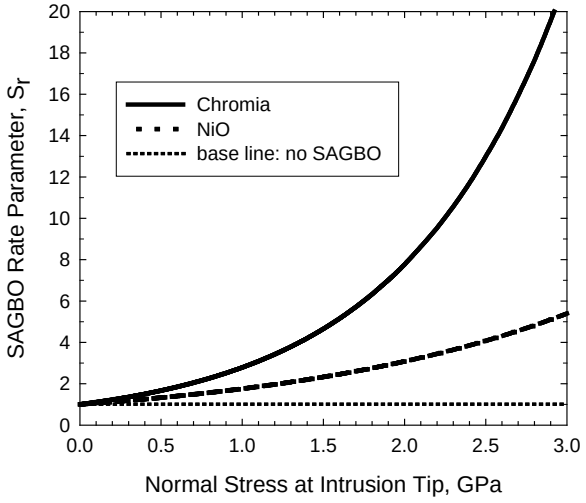

Figure 11: The dependence of the calculated SAGBO rate parameter, S_r, on tensile stress at the tip of the oxide intrusion for chromia and nickel oxide at 650°C [87].

The calculations show that the SAGBO parameter will be higher for chromia than for NiO and this is in agreement with the observations of Kitaguchi et al. [82] in terms of intrusion length. Furthermore, a value of ~2.5 GPa for the normal stress at the intrusion tip produces values of S_r similar to those found experimentally [82], again in terms of intrusion length (17.6 for chromia and 3.6 for NiO). This level of stress is not unreasonable for the strong RR1000 specimens examined by Taniguchi but it is also the case that microstructural changes or creep processes that weaken the alloy are likely to reduce the SAGBO enhancement factor [88] even though oxide intrusions form at the crack tip. Generally, it

can be appreciated from Figure 11, that in weaker alloys the experimental demonstration of the SAGBO phenomenon may prove elusive.

Conclusions

Chromia-forming Ni-based superalloys are widely used as structural components and, particularly, as turbine discs at temperatures up to ~750^{o}C. There is increasing demand for operation at even higher temperatures, say to 800^{o}C, and this places emphasis on the oxidation resistance of the alloys and the interaction of oxidation with mechanical properties. This overview examines these aspects. It is shown that, in addition to the formation of a surface layer of chromia, typical alloys are also internally oxidised to form, principally, alumina and this results in the development of intergranular intrusions of alumina of acicular appearance, discrete intragranular precipitates and a surface zone depleted of γ'. Shot-peening the alloy surface does not affect these broad trends although detailed differences in the morphology of the internal oxides and recrystallization of the surface regions can occur.

Low alloy titanium content appears to have a beneficial effect on oxidation resistance whereas high contents result in the formation of discrete crystals of rutile above the surface chromia layer. This has been known for many years but more recent studies have shown that titanium also increases the growth rate of the chromia layer itself. This is attributed to the doping of the Cr sub-lattice with 4-valent Ti ions and the creation of extra vacancies that increase Cr diffusion rates within its oxide and, consequently, oxidation rates. This oxidation enhancement is highest in the early stages of oxidation but declines with time as the near-surface concentration of Ti becomes depleted.

There is currently a lack of clarity on the influence of applied loads on oxidation behaviour. This arises because of uncertainty in the stress levels, and their sign, present in the oxide layers. Allowances have not been made for intrinsic growth stresses, the redistribution of the applied load between oxide and alloy and, in some cases, cooling stresses. As a result, quantitative assessment is not possible although tensile cracking and localised oxide spallation are evident and both lead to enhanced oxidation rates. Similarly, the cracking of the surface oxides and/or the immediate sub-surface alumina penetrations provide nucleation sites for fatigue crack development.

The growth rate of fatigue cracks in air is very much larger than under inert atmospheres. Recent TEM observations indicate that this oxygen effect is associated with the development and cracking of oxide intrusions emanating from the crack tip and penetrating along the alloy grain boundary. The growth rate of these intrusions can be an order of magnitude larger than expected and this may be

evidence of stress aided grain boundary oxidation (SAGBO) although experimental data are limited. It is expected that the formation of typical oxides (NiO, chromia) at the crack tip will perturb the stress field such that out-of-plane normal stresses there can become compressive and then rise to tensile at the tip of the intrusion. This modified stress distribution has not yet been quantified but has been incorporated into a recent model of SAGBO.

References

[1] T.P. Gabb, J. Telesman, P.T. Kantzos, J.W. Smith, P.F. Browning, Effects of high temperature exposures on fatigue life of disk superalloys, Superalloys 2004, (2004) 269-274.

[2] J. Gayda, R.V. Miner, Fatigue crack initiation and propagation in several nickel-base superalloys at 650°C, International Journal of Fatigue, 5 (1983) 135-143.

[3] R.L. Kennedy, Allvac 718plus, superalloy for the next forty years, in: E.A. Loria (Ed.) Superalloys 718, 625, 706 and derivatives 2005, TMS, USA, 2005.

[4] R. Reed, The Superalloys: Fundamentals and applications, in, Cambridge university press, Cambridge, 2006.

[5] J. Chen, P. Rogers, J.A. Little, Oxidation behavior of several chromia-forming commercial nickel-base superalloys, Oxidation of Metals, 47 (1997) 381-410.

[6] A. Encinas-Oropesa, G.L. Drew, M.C. Hardy, A.J. Leggett, J.R. Nicholls, N.J. Simms, Effects of oxidation and hot corrosion in a nickel disc alloy, in: Superalloys 2008: 11th International Symposium on Superalloys TMS, 2008, pp. 609-618.

[7] A. Encinas-Oropesa, N.J. Simms, J.R. Nicholls, G.L. Drew, J. Leggett, M.C. Hardy, Evaluation of oxidation related damage caused to a gas turbine disc alloy between 700 and 800°C, Materials at High Temperatures, 26 (2009) 241-249.

[8] J.L. Evans, Effect of surface roughness on the oxidation behavior of the Ni-base superalloy ME3, Journal of Materials Engineering and Performance, 19 (2010) 1001-1004.

[9] D. Kim, C. Jang, W. Ryu, Oxidation characteristics and oxide layer evolution of Alloy 617 and Haynes 230 at 900 °C and 1100 °C, Oxidation of Metals, 71 (2009) 271-293.

[10] F.A. Khalid, N. Hussain, K.A. Shahid, Microstructure and morphology of high temperature oxidation in superalloys, Materials Science and Engineering: A, 265 (1999) 87-94.

[11] G.A. Greene, C.C. Finfrock, Oxidation of Inconel 718 in Air at High Temperatures, Oxidation of Metals, 55 (2001) 505-521.

[12] L. Zheng, M. Zhang, J. Dong, Oxidation behavior and mechanism of powder metallurgy Rene95 nickel based superalloy between 800 and 1000 °C, Applied Surface Science, 256 (2010) 7510-7515.

[13] K. Al-Hatab, M. Al-Bukhaiti, U. Krupp, M. Kantehm, Cyclic oxidation behavior of IN 718 Superalloy in air at high temperatures, Oxidation of Metals, 75 (2011) 209-228.

[14] S. Cruchley, H.E. Evans, M.P. Taylor, M.C. Hardy, S. Stekovic, Chromia layer growth on a Ni-based superalloy: Sub-parabolic kinetics and the role of titanium, Corrosion Science, 75 (2013) 58-66.

[15] C.K. Sudbrack, S.L. Draper, T.T. Gorman, J. Telesman, T.P. Gabb, D.R. Hull, Oxidation and the effects of high temperature exposures on notched fatigue life of an advanced powder metallurgy disk superalloy, in: E.S. Huron, R.C. Reed, M.C. Hardy, M.J. Mills, R.E. Montero, P.D. Portella, J. Telesman (Eds.) Superalloys 2012: 12th International Symposium on Superalloys, TMS, Seven Springs, PA, 2012, pp. 863-872.

[16] M.P. Taylor, H.E. Evans, S. Stekovic, M.C. Hardy, The oxidation characteristics of the Ni-base superalloy, RR1000, at temperatures 700-900^{o}C, Materials at High Temperatures, 29 (2012) 145-150.

[17] S. Cruchley, M.P. Taylor, R. Ding, H.E. Evans, D.J. Child, M.C. Hardy, Comparison of chromia growth kinetics in a Ni-based superalloy, with and without shot-peening, Corrosion Science, 100 (2015) 242-252.

[18] S. Cruchley, M.P. Taylor, H.E. Evans, M.C. Hardy, D.J. Child, Characterisation of subsurface oxidation damage in Ni based superalloy, RR1000, Materials Science and Technology, 30 (2014) 1884-1889.

[19] S. Cruchley, M.P. Taylor, H.E. Evans, P. Bowen, M.C. Hardy, S. Stekovic, Microstructural characterisation of high temperature oxidation of nickel Base Superalloy RR1000 and the effect of shot-peening, in: E.S. Huron, R.C. Reed, M.C. Hardy, M.J. Mills, R.E. Montero, P.D. Portella, J. Telesman (Eds.) Superalloys 2012: 12th International Symposium on Superalloys, TMS, Seven Springs, PA, 2012, pp. 751-758.

[20] G.C. Wood, T. Hodgkiess, D.P. Whittle, A comparison of the scaling behaviour of pure iron-chromium and nickel-chromium alloys in oxygen, Corrosion Science, 6 (1966) 129-147.

[21] I.M. Edmonds, H.E. Evans, C.N. Jones, The role of γ' precipitate dispersion in forming a protective scale on Ni-based superalloy at 750^{o}C, Oxidation of Metals, 73 (2012) 193-206.

[22] J. Issartel, S. Martoia, F. Charlot, V. Parry, G. Parry, R. Estevez, Y. Wouters, High temperature behavior of the metal/oxide interface of ferritic stainless steels, Corrosion Science, 59 (2012) 148-156.

[23] H. Ackermann, G. Teneva-Kosseva, K. Lucka, H. Koehne, S. Richter, J. Mayer, Oxidation behaviour of selected wrought Ni-base high temperature alloys when used as flame tube material in modern blue flame oil burners, Corrosion Science, 49 (2007) 3866-3879.

[24] D.J. Young, Predicting internal oxidation: Building on the wagner model. , Materials Science Forum, 969 (2011) 1-11.

[25] P. Huszkowski, S. Ertl, J. Piron-Abellan, N. Christiansen, T. fler, V. Shemet, L. Singheiser, W.J. Quadakkers, Effect of component thickness on lifetime and oxidation rate of chromia forming ferritic steels in low and high pO_2 environments, Materials at High Temperatures, 22 (2005) 253-262.

[26] B.J. Foss, M.C. Hardy, D.J. Child, D.S. McPhail, B.A. Shollock, Oxidation of a Commercial Nickel-Based Superalloy under Static Loading, JOM, 66 (2014) 2516-2524.

[27] R.J. Mitchell, C.M. Rae, S. Tin, Grain boundary transformations during isothermal exposure of powder metallurgy nickel base superalloys for turbine disc applications, Materials Science and Technology, 21 (2005) 125-132.

[28] H.E. Evans, D.A. Hilton, R.A. Holm, Internal attack during the oxidation of nitrided stainless steels, Oxidation of Metals, 11 (1977) 1-21.

[29] Y. Shida, G.C. Wood, F.H. Stott, D.P. Whittle, B.D. Bastow, Intergranular oxidation and internal void formation in Ni-40%Cr alloys, Corr. Sci., 21, (1981), 581-597.

[30] S. Cruchley, J.F. Sun, M.P. Taylor, H.E. Evans, P. Bowen, J. Sumner, J.R. Nicholls, N.J. Simms, B.A. Shollock, R.J. Chater, B.J. Foss, M.C. Hardy, S. Stekovic, Cautionary note on use of focused ion beam sectioning as technique for characterising oxidation damage in Ni based superalloys, Materials at High Temperatures, 31 (2014) 27-33.

[31] H.E. Evans, D.A. Hilton, R.A. Holm, S.J. Webster, Influence of a titanium nitride dispersion on the oxidation behaviur of 20%Cr 25%Ni stainless steel, Oxidation of Metals, 12 (1978) 473-485.

[32] B.R. Barnard, P.K. Liaw, R.A. Buchanan, D.L. Klarstrom, Affects of applied stresses on the isothermal and cyclic high-temperature oxidation behavior of superalloys, Materials Science and Engineering: A, 527 (2010) 3813-3821.

[33] H.E. Evans, A.T. Donaldson, T.C. Gilmour, Mechanisms of breakaway oxidation and application to a chromia-forming steel, Oxidation of Metals, 52 (1999) 379-402.

[34] P.J. Ennis, W.J. Quadakkers, Corrosion and creep of nickel-base alloys in steam reforming gas, in: J.B. Marriott, M. Merz, J. Nihoul, J. Ward (Eds.) High Temperature Alloys, Springer Netherlands, 1988, pp. 465-474.

[35] A.N. Blacklocks, A. Atkinson, R.J. Packer, S.L.P. Savin, A.V. Chadwick, An XAS study of the defect structure of Ti-doped α-Cr_2O_3, Solid State Ionics, 177 (2006) 2939-2944.

[36] A. Atkinson, M.R. Levy, S. Roche, R.A. Rudkin, Defect properties of Ti-doped Cr_2O_3, Solid State Ionics, 177 (2006) 1767-1770.

[37] R. Naraparaju, H.J. Christ, F. Renner, A. Kostka, Effect of shot-peening on the oxidation behaviour of boiler steels, Oxidation of Metals, (2011) 1-13.

[38] R. Naraparaju, H.J. Christ, F.U. Renner, A. Kostka, Dislocation engineering and its effect on the oxidation behaviour, Materials at High Temperatures, 29 (2012) 116-122.

[39] J.C. Rosser, M.I. Bass, C. Cooper, T. Lant, P.D. Brown, B.J. Connolly, H.E. Evans, Steam oxidation of Super 304H and shot-peened Super 304H, Materials at High Temperatures, 29 (2012) 95-106.

[40] Y. Zengwu, F. Min, W. Xuegang, L. Xingeng, Effect of shot-peening on the oxidation resistance of TP304H and HR3C steels in water vapor, Oxidation of Metals, (2011) 1-10.

[41] L. Tan, X. Ren, K. Sridharan, T.R. Allen, Effect of shot-peening on the oxidation of alloy 800H exposed to supercritical water and cyclic oxidation, Corrosion Science, 50 (2008) 2040-2046.

[42] A.S. Khanna, J.B. Gnanamoorthy, Effect of cold work on the oxidation resistance of 2.25Cr-1 Mo steel, Oxidation of Metals, 23 (1985) 17-33.

[43] M. Warzee, J. Hennaut, M. Maurice, C. Sonnen, J. Waty, P. Berge, Effect of surface treatment on the corrosion of stainless steels in high-temperature water and steam, Journal of The Electrochemical Society, 112 (1965) 670-674.

[44] A.M. Huntz, B. Lefevre, F. Cassino, Roughness and oxidation: application to NiO growth on Ni at 800°C, Materials Science and Engineering: A, 290 (2000) 190-197.

[45] S. Uran, B. Veal, M. Grimsditch, J. Pearson, A. Berger, Effect of surface roughness on oxidation: Changes in scale thickness, composition, and residual stress, Oxidation of Metals, 54 (2000) 73-85.

[46] Z.G. Zhang, P.Y. Hou, F. Gesmundo, Y. Niu, Effect of surface roughness on the development of protective Al_2O_3 on Fe–10Al (at.%) alloys containing 0–10 at.% Cr, Applied Surface Science, 253 (2006) 881-888.

[47] J.E. Tang, M. Halvarsson, H. Asteman, J.E. Svensson, Microstructure of oxidised 304L steel and the effects of surface roughness on oxidation behaviour, Materials Science Forum, 369-372 (2001) 205-214.

[48] M.P. Taylor, H.E. Evans, S. Stekovic, M.C. Hardy, The Oxidation Characteristics of the Ni-base Superalloy, RR1000, at Temperatures 700-900^{o}C, in: G.J. Tatlock, H.E. Evans (Eds.) Microscopy of Oxidation 8, Liverpool, 2011.

[49] D.J. Child, G.D. West, R.C. Thomson, Assessment of surface hardening effects from shot peening on a Ni-based alloy using electron backscatter diffraction techniques, Acta Materialia, 59 (2011) 4825-4834.

[50] B.J. Foss, S. Gray, M.C. Hardy, S. Stekovic, D.S. McPhail, B.A. Shollock, Analysis of shot-peening and residual stress relaxation in the nickel-based superalloy RR1000, Acta Materialia, 61 (2013) 2548-2559.

[51] W. Dong, H.E. Bishop, D, Johnson, D.G. Lees, G.W. Lorimer, An investigation of the growth mechanism of scale formed on chromium containing low amounts of sulfur, chlorine and phosphorus, Oxid. Metals, 54 (2000) 509-525.

[52] C.H. Zhou, H.T. Ma, L. Wang, Comparative study of oxidation kinetics for pure nickel oxidized under tensile and compressive stress, Corrosion Science, 52 (2010) 210-215.

[53] C. Zhou, H. Ma, L. Wang, Effect of mechanical loading on the oxidation kinetics and oxide-scale failure of pure Ni, Oxidation of Metals, 70 (2008) 287-294.

[54] G. Moulin, P. Arevalo, A. Salleo, Influence of external mechanical loadings (creep, fatigue) on oxygen diffusion during nickel oxidation, Oxidation of Metals, 45 (1996) 153-181.

[55] A. Karabela, L.G. Zhao, J. Tong, N.J. Simms, J.R. Nicholls, M.C. Hardy, Effects of cyclic stress and temperature on oxidation damage of a nickel-based superalloy, Materials Science and Engineering: A, 528 (2011).

[56] J.H. O'Hanlon, M.C. Hardy, D.J. Child, B.J. Foss, P.J. Withers, M.R. Bache, The effect of minimum dwell cycles on the environmental and fatigue response of RR1000, in: MATEC WEB OF CONFERENCES 14 :04003 2014.

[57] M. Reger, L. Remy, Fatigue oxidation interaction in IN-100 superalloy Metallurgical Transactions A - Physical Metallurgy and Materials Science, 19 (1988) 2259-2268.

[58] M. Schütze, The healing behavior of protective oxide scales on heat-resistant steels after cracking under tensile strain, Oxidation of Metals, 25 (1986) 409-421.

[59] M.M. Nagl, S.R.J. Saunders, W.T. Evans, D.J. Hall, The tensile failure of nickel oxide scales at ambient and at growth temperature, Corrosion Science, 35 (1993) 965-977.

[60] M.P. Taylor, H.E. Evans, E.P. Busso, Z.Q. Qian, Creep properties of a Pt–aluminide coating, Acta Materialia, 54 (2006) 3241-3252.

[61] M.P. Taylor, H.E. Evans, C.B. Ponton, J.R. Nicholls, A method for evaluating the creep properties of overlay coatings, Surface and Coatings Technology, 124 (2000) 13-18.

[62] I.A. Menzies, K.N. Strafford, Observations on the mechanical properties of nickel oxide scales, J Mater Sci, 2 (1967) 358-364.

[63] T.P. Gabb, J. Telesman, P.T. Kantzos, J.W. Smith, P.F. Browning, Effects of high temperature exposures on fatigue life of disk superalloys, in: K.A. Green, T.M. Pollock, H. Harada, T.E. Howson, R.C. Reed, J.J. Schirra, S. Walston (Eds.) Superalloys 2004: 10th international symposium on superalloys, TMS, Seven Springs, PA, 2004, pp. 269-274.

[64] A.M. Huntz, C. Liu, M. Kornmeier, J.L. Lebrun, The determination of stresses during oxidation of Ni: in situ measurements by XRD at high temperature, Corrosion Science, 35 (1993) 989-997.

[65] S. Gray, K. Berriche-Bouhanek, H.E. Evans, Oxide growth stresses in an austenitic stainless steel determined by creep extension, Materials Science Forum, 461-464 (2004) 755-762.

[66] A. Pineau, D.L. McDowell, E.P. Busso, S.D. Antolovich, Failure of metals II: Fatigue, Acta Materialia, (2015).

[67] H.E. Evans, Stress effects in high temperature oxidation of metals, International Materials Reviews, 40 (1995) 1-40.

[68] S. Cruchley, H.Y. Li, H.E. Evans, P. Bowen, D.J. Child, M.C. Hardy, The Role of oxidation damage in fatigue crack Initiation of an advanced Ni-based superalloy, International Journal of Fatigue, 81 (2015) 265-274.

[69] S. Cruchley, M.P. Taylor, H.Y. Li, P. Bowen, D.J. Child, M.C. Hardy, Effect of prior oxidation on high cycle fatigue performance of RR1000 and the role of oxidation in fatigue crack initiaiton, Materials at High Temperatures, 31 (2015) 68-73.

[70] S.D. Antolovich, P. Domas, J.L. Strudel, Low cycle fatigue of René 80 as affected by prior exposure, Metallurgical Transactions A - Physical Metallurgy and Materials Science, 10 (1979) 1859-1868.

[71] R. Jiang, S. Everitt, N. Gao, K. Soady, J.W. Brooks, P.A.S. Reed, Influence of oxidation on fatigue crack initiation and propagation in turbine disc alloy N18, International Journal of Fatigue, 75 (2015) 89-99.

[72] D.A. Woodford, Gas phase embrittlement and time dependent cracking of nickel based superalloys, Energy Materials, 1 (2006) 59-79.

[73] G. Onofrio, G.A. Osinkolu, M. Marchionni, Fatigue crack growth of UDIMET 720 Li superalloy at elevated temperature, International Journal of Fatigue, 23 (2001) 887-895.

[74] M. Marchionni, G.A. Osinkolu, G. Onofrio, High temperature low cycle fatigue behaviour of UDIMET 720 Li superalloy, International Journal of Fatigue, 24 (2002) 1261-1267.

[75] L. Coffin Jr, Fatigue at high temperature, in: Fatigue at Elevated Temperatures, ASTM STP, 1973, pp. 5-34.

[76] R. Jiang, S. Everitt, M. Lewandowski, N. Gao, P.A.S. Reed, Grain size effects in a Ni-based turbine disc alloy in the time and cycle dependent crack growth regimes, International Journal of Fatigue, 62 (2014) 217-227.

[77] K.S. Chan, A Grain Boundary Fracture Model for Predicting Dynamic Embrittlement and Oxidation-Induced Cracking in Superalloys, Metall and Mat Trans A, 46 (2015) 2491-2505.

[78] U. Krupp, W.M. Kane, C. Laird, C.J. McMahon, Brittle intergranular fracture of a Ni-base superalloy at high temperatures by dynamic embrittlement, Materials Science and Engineering A, 387-389 (2004) 409-413.

[79] J.A. Pfaendtner, C.J. McMahon Jr, Oxygen-induced intergranular cracking of a Ni-base alloy at elevated temperatures--an example of dynamic embrittlement, Acta Materialia, 49 (2001) 3369-3377.

[80] R.H. Bricknell, D.A. Woodford, The embrittlement of nickel following high temperature air exposure, MTA, 12 (1981) 425-433.

[81] R.H. Bricknell, D.A. Woodford, The mechanism of cavity formation during high temperature oxidation of nickel, Acta Metallurgica, 30 (1982) 257-264.

[82] H.S. Kitaguchi, H.Y. Li, H.E. Evans, R.G. Ding, I.P. Jones, G. Baxter, P. Bowen, Oxidation ahead of a crack tip in an advanced Ni-based superalloy, Acta Materialia, 61 (2013) 1968-1981.

[83] E. Andrieu, R. Molins, H. Ghonem, A. Pineau, Intergranular crack tip oxidation mechanism in a nickel-based superalloy, Materials Science and Engineering: A, 154 (1992) 21-28.

[84] H.W. Liu, Y. Oshida, Grain boundary oxidation and fatigue crack growth at elevated temperatures, Theoretical and Applied Fracture Mechanics, 6 (1986) 85-94.

[85] H.S. Kitaguchi, M.P. Moody, H.Y. Li, H.E. Evans, M.C. Hardy, S. Lozano-Perez, An atom probe tomography study of the oxide–metal interface of an oxide intrusion ahead of a crack in a polycrystalline Ni-based superalloy, Scripta Materialia, 97 (2015) 41-44.

[86] L. Viskari, M. Hörnqvist, K.L. Moore, Y. Cao, K. Stiller, Intergranular crack tip oxidation in a Ni-base superalloy, Acta Materialia, 61 (2013) 3630-3639.

[87] H.E. Evans, H.Y. Li, P. Bowen, A mechanism for stress-aided grain boundary oxidation ahead of cracks, Scripta Materialia, 69 (2013) 179-182.

[88] H.Y. Li, J.F. Sun, M.C. Hardy, H.E. Evans, S.J. Williams, T.J.A. Doel, P. Bowen, Effects of microstructure on high temperature dwell fatigue crack growth in a coarse grain PM nickel based superalloy, Acta Materialia, 90 (2015) 355-369.

List of Figure Captions

Figure 1: Oxidation of Ni-based superalloy, ME3, exposed to air at 815^{o}C for 2020 hours, showing an external layer of Cr_2O_3 externally with an internal oxidation zone of Al_2O_3 [15]. See text for fuller discussion.

Figure 2: Arrhenius plot of kp values from the literature of similar Ni-based superalloys used for rotor disc applications and typical expected behaviour for chromia formation on a high chromium containing austenitic stainless steel (dashed line) [5, 7, 11, 12, 31, 32]. Image modified from Cruchley et al. (2013) to include data taken from [17].

Figure 3: Plot of chromia thickness measured on RR1000, with and without shot-peening, at 750^{o}C compared with Ti-free austenitic steel/pure chromium. Oxide measurements for both conditions were normally distributed and error bars are shown as ± 1 standard deviation. Hollow squares are measurements for shot-peened RR1000, filled circles are polished RR1000 [17].

Figure 4: The variation of the enhancement ratio of the chromia growth rate due to Ti doping with oxide thickness for 700^{o}C, 750^{o}C and 800^{o}C, in a) polished RR1000 and b) shot-peened RR1000 [17].

Figure 5: Comparison of the oxidation damage formed on a) polished RR1000 and b) shot-peened RR1000 oxidised for 2000 hours at 700^{o}C [17].

Figure 6: Backscatter electron images of oxidation damage on fine-grained RR1000 after 200 hours at 700^{o}C under hold stresses of (a) + 600 MPa, (b) 0 MPa and (c) −600 MPa [56].

Figure 7: BSE image of an etched pre-oxidised (2000h, 700^{o}C) specimen that failed after 1.9x10^{6} cycles during room temperature 4-point bend at a maximum applied stress of 800 MPa, showing cracking of the external and intergranular internal oxide along with the presence of both a γ′ denuded zone and carbide dissolution zone [68].

Figure 8: Comparison of the mean notched fatigue lives at 704°C of the unexposed ME3 specimens and ME3 specimens with a) prior exposures in air and b) alternative conditions as marked. Diamonds are each test result, clearly showing that the removal of all of the environmental damage (50 μm removal) leads to a full restoration in fatigue life [15].

Figure 9: Main graph shows crack growth rates versus ΔK in the LHSR alloy tested under 3-point bend at 650°C (black symbols) and 725°C (red symbols) under air and vacuum. Increased rates were observed in air at both temperatures but were greater at the higher temperature. Micrograph (a) shows the intergranular fracture behaviour at 725°C in air and (b) the transgranular behaviour in vacuum both at $\Delta K \sim 40$ MPa.m$^{-½}$ [76].

Figure 10: A bright field STEM image, EDX maps and linescans obtained ahead of the crack tip in RR1000, illustrating the presence and sequence of oxides. The relative concentration in the EDX maps increases from low to high in the sequence: black, blue, green, yellow, orange and red [82].

Figure 11: The dependence of the calculated SAGBO rate parameter, Sr, on tensile stress at the tip of the oxide intrusion for chromia and nickel oxide at 650°C [87].

List of Table Captions

Table 1: Compositions of some representative alloys [1-4].